Journal of Membrane Science 516 (2016) 152–161

Contents lists available at ScienceDirect

Journal of Membrane Science

journal homepage: www.elsevier.com/locate/memsci

Understanding the role of nanoparticle size and polydispersity in fouling development during dead-end microfiltration

Krzysztof Trzaskus, Mariël Elshof, Antoine Kemperman *, Kitty Nijmeijer

Membrane Science & Technology, MESA+ Institute for Nanotechnology, University of Twente, Faculty of Science and Technology, P.O. Box 217, 7500 AE Enschede, The Netherlands

ARTICLE INFO

Article history:
Received 8 January 2016
Received in revised form
13 May 2016
Accepted 26 May 2016
Available online 6 June 2016

Keywords:
Nanoparticle size
Polydispersity
Microfiltration
Silica
Fouling

ABSTRACT

The recent exponential growth of nanotechnology and numerous applications of nanotechnology-based products resulted in water pollution by engineered nanoparticles. Over the last few decades, membrane technology has emerged as one of the most promising and reliable techniques in water purification. Therefore, it is an obvious candidate to remove manufactured nano-sized contaminants and to purify the water. Nanoparticle properties play a crucial role in the performance and effectiveness of membrane filtration.

This experimental study investigates the role of nanoparticle size and polydispersity on fouling and rejection development during dead-end microfiltration of electrostatically stabilized silica nanoparticles. Our work on filtration of monodisperse silica nanoparticles (11 nm, 25 nm and 92 nm) smaller than the membrane pore size (~200 nm) demonstrates that an increasing nanoparticle diameter accelerates pore blockage and development of cake. The specific cake resistance of the filtration cake formed decreases with increasing nanoparticle diameter. Filtration of polydisperse nanoparticles (obtained by mixing monodisperse suspensions in various ratios) shows that increasing the fraction of smaller nanoparticles results in delayed pore blockage, and cake filtration occurring at a later stage. The specific cake resistance of the polydisperse nanoparticles is always found to be in between that obtained for the monodisperse nanoparticle suspensions. An increasing weight fraction of larger nanoparticles results in faster development of nanoparticle rejection due to accelerated pore blockage. However, because of the highly porous structure of the filtration cake originating from strong surface charges, the moderate transmembrane pressure applied and cake imperfections, the smallest (11 nm) nanoparticles were rejected only to a low extent, even during the cake filtration stage. An increase in applied transmembrane pressure during filtration of the polydisperse suspension resulted in faster pore blockage and higher specific cake resistance. Nevertheless, rejection of the nanoparticles in the cake filtration stage improved only slightly with increasing transmembrane pressure.

1. Introduction

Increasing production of engineered nanoparticles results in their accumulation in drinking water sources [1–4]. Due to their size range, nanoparticles are classified as colloidal particles, which can be effectively removed by membranes [5–7]. However, to date inevitable fouling phenomena reducing membrane performance limits the widespread usage of membrane technology in water purification [8,9]. Even though the backgrounds of fouling phenomena are rather well understood, the various kinds of feed solutions, membranes and filtration modes make an accurate prediction of the fouling behavior in the case of nanoparticles challenging yet.

Nanoparticle rejection is not only determined by the ratio between the membrane pore size and the nanoparticle size, but also electrostatic or steric repulsion effects between solute and membrane material determine to a large extent the retention [10]. Furthermore, pore blocking and/or concentration polarization phenomena occurring during the filtration may change nanoparticle rejection [11,12]. Due to a combination of those effects, as shown in our previous work [13], membranes with much bigger pores than the nanoparticle diameter can still reject nanoparticles. We have shown that during dead-end filtration of a stable nanoparticle suspension with membrane pores much bigger than the nanoparticle diameter, fouling develops in five stages: 1) nanoparticle adsorption onto the membrane, 2) transport through the membrane pores, 3) pore blocking, 4) cake filtration, and 5) cake maturation (see Fig. 1(a)). Due to pore blockage and formation of a nanoparticle deposit on the membrane surface acting as a dynamic

* Corresponding author.
E-mail address: a.j.b.kemperman@utwente.nl (A. Kemperman).

http://dx.doi.org/10.1016/j.memsci.2016.05.043
0376-7388/

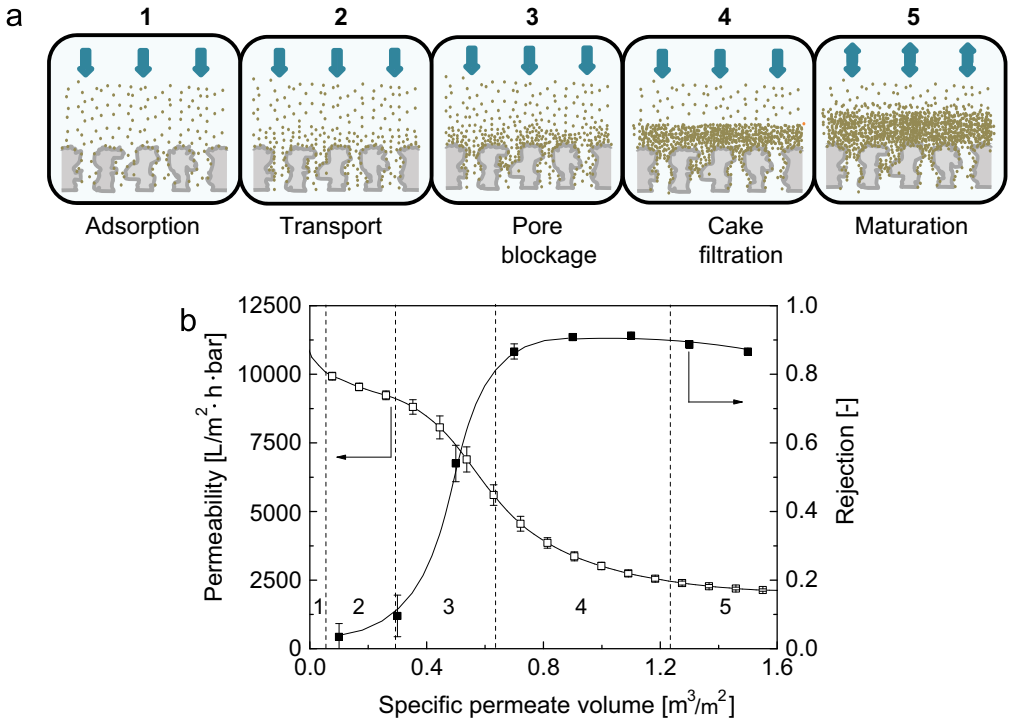

Fig. 1. (a) Fouling mechanism of the membrane during dead-end microfiltration of nanoparticles much smaller than the membrane pore size; (b) Permeability and rejection of silica nanoparticles as a function of the specific permeate volume during dead-end microfiltration of 2 mg/L Ludox TM-50 silica nanoparticles (adapted from [13]).

secondary membrane, further transport of the nanoparticles through the membrane is limited. As a result, nanoparticle rejection also increases significantly during the course of the filtration, as shown in Fig. 1(b).

Although our previous work describes filtration of a monodisperse model nanoparticles suspension, in practice real feed waters contain nanoparticles of various sizes resulting in a more complex filtration behavior. This justifies the further investigation of the role of nanoparticle polydispersity on membrane filtration performance and fouling behavior.

Several studies proved that the resistance of the filtration cake formed by polydisperse suspensions is different from that obtained for monodisperse solutions [14,15]. McDonogh et al. [16] studied the influence of nanoparticle polydispersity on the formation of the nanoparticle deposit. They showed that increasing polydispersity of the charged nanoparticles resulted in a more porous and less ordered cake structure. Kim and Ng [17] showed that polydisperse nanoparticles form a denser filtration cake when a greater number of smaller nanoparticles was present in the feed solution.

To the best of our knowledge, there are no systematic studies carried out on the determination of the role of nanoparticle polydispersity in fouling development resulting in pore blockage and subsequent cake filtration. In this paper the effect of nanoparticle size and size distribution on fouling and rejection development is investigated. The use of a controlled size distribution of nanoparticles in the feed solution, combined with extensive filtration data, allow the determination of the mechanisms responsible for fouling and nanoparticle rejection of polydisperse nanoparticles in dead-end microfiltration.

2. Experimental

2.1. Materials

Colloidal silica Ludox TM-50 (50% w/w), Ludox SM (30% w/w) (both from Sigma Aldrich) and Levasil 30/50 (50% w/w) (AkzoNobel), which vary in average nanoparticle size, were provided as a water suspension. ACS grade NH_4HCO_3, $(NH_4)_2CO_3$, HCl and NaOH (Sigma Aldrich) were applied to adjust the pH and ionic strength of the colloidal suspensions used. All chemicals were used without further purification; all solutions were prepared using ultrapure Milli-Q water (resistivity $>18.2\ M\Omega\cdot cm$).

2.2. Feed and permeate characterization

The surface zeta potential of the silica nanoparticles were measured by electrophoretic mobility measurements using a Malvern ZetaSizer 3000Hsa. The measurements were carried out with a 0.5 g/L nanoparticles suspension with pH 8, prepared by dilution of the commercial suspensions in Milli-Q water. Transmission Electron Microscope (TEM) images of silica nanoparticles in the stock suspensions were obtained using a Philips CM300ST-FEG microscope. The number size distribution of each nanoparticle type was determined from the TEM images using ImageJ 1.48v software (National Institute of Health). We used a Scanning Mobility Particle Sizer (SMPS) model 3936 to measure the particle size distribution in the feed and permeate samples. The SMPS consisted of an electrostatic classifier model 3080, a neutralizer model 3077 with a Krypton-85 source (370MBq), a nano DMA model 3085 and a butanol based Condensation Particle Counter (CPC) model 3025A, all from TSI Incorporated (USA). The SMPS combined particle size classification according to the particle mobility diameter with measurement of the concentration using a CPC [18]. Briefly, nanoparticles firstly were aerosolized by with Electrospray Aerosol Generator model 3480. Electrical mobility of the nanoparticles in air is size dependent, and this mobility was measured by SMPS model 3936. The system was adjusted to a size range between 10 nm and 100 nm, a scan time of 95 s, a retrace time of 15 s, and a two minute recurrence interval.

2.3. Membrane and membrane characterization

We used a commercial Pentair X-Flow 1.5MF02 inside/out hollow fiber membrane (OD 2.4 mm, ID 1.5 mm, kindly provided

by Pentair X-Flow BV, the Netherlands), in all filtration experiments. The membrane was characterized in terms of pore size distribution (with capillary flow porometry), surface zeta potential (using streaming potential measurements) and clean water permeability. Detailed description of the filtration module preparation and membrane characterization was described in details elsewhere [13].

The properties of the MF membrane used are shown in Table 1. These data are taken from our previous study [13]. The clean water permeability of the membrane was about $11.5 \pm 0.5 \cdot 10^3$ L/m^2 h bar. The average mean flow pore diameter measured with capillary flow porometry was found to be 200 ± 15 nm. The inside (lumen) surface of the membrane is negatively charged at pH 8 with zeta potential of -23.1 ± 2.1 mV.

2.4. Filtration experiments and data processing

We conducted all filtration experiments in a constant pressure filtration setup, assembled according to Fig. 2.

A detailed description of the experimental procedure was given in our previous study [13]. Briefly, a single filtration experiment consists of Milli-Q water filtration (50 mL) followed by nanoparticle filtration (400 mL of the feed solution). Continuous cumulative mass increment was recorded by an analytical balance connected to the computer. The permeability was calculated according to Eq. (1):

$$L_p = \frac{J}{\Delta P} \tag{1}$$

where L_p is the liquid permeability (L/m^2 h bar), J is the flux (L/m^2 h), and ΔP is the transmembrane pressure (bar). Every 50 mL, permeate samples were collected and the silicon content in the samples was analyzed by ICP-MS (Inductively Coupled Plasma Mass Spectrometry, Thermo Fisher Xseries 2). Rejection of the silica nanoparticles was calculated according to Eq. (2):

$$\sigma = 1 - \frac{C_P}{C_f} \tag{2}$$

where σ is the rejection (−), C_P is the concentration of the nanoparticles in the permeate sample (mg/L), and C_f is the concentration of the nanoparticles in the feed solution (mg/L).

Due to the asymmetric structure of the membrane applied, pore blockage occurred only in a thin selective layer of the membrane. As a result, contribution of the pore blockage to the filtration resistance was limited [13]. Therefore, the filtration resistance originated mainly from the nanoparticle deposition on the membrane surface in form of a filtration cake. Formation of this cake leads to a reduction of the permeate flux and can be described using Eq. (3):

$$J = \frac{\Delta P}{\eta \cdot (R_m + R_c)} \tag{3}$$

where η is the viscosity (Pa s), R_m is the membrane resistance (1/m) and R_c is the additional resistance caused by deposition of nanoparticles on the membrane (1/m) as a cake, defined as:

$$R_c = \alpha \frac{m_p}{A} \tag{4}$$

Here, α is the specific cake resistance (m/kg), m_p is the mass of the filtration cake deposited on the membrane surface (kg), and A is the membrane area (m^2). The specific cake resistance α quantitatively describes compaction of the cake layer. The resistance caused by nanoparticle deposit is linked to the porosity of the filtration cake and nanoparticle size with Kozeny–Carman equation [21], defined as:

$$R_c = 180 \cdot \frac{m_p}{d_p^2 A \rho_p} \frac{(1-\epsilon)}{\epsilon^3} \tag{5}$$

where R_c is the filtration cake resistance (1/m), m_p is the mass of the filtration cake (kg), A is the membrane area (m^2), ρ_p is the density of the solute (kg/m^2), d_p the diameter of the spherical particle (m) and ε the porosity of the filtration cake (−).

The cake compression increases with applied transmembrane pressure, often estimated in terms of empirical power-law function as [19]:

$$\alpha = \alpha_0 (\Delta P)^s \tag{6}$$

where α_0 is a constant related to the size and shape of the particles (m/kg)/(Pa)^s, and s is the compressibility coefficient (−), which varies from 0 for an incompressible cake to a value near 1 for a highly compressible cake.

To investigate the role of the nanoparticle size and polydispersity in dead-end microfiltration, we prepared and filtered Milli-Q water solutions containing 1 mM ammonium bicarbonate buffer and 2 mg/L of silica nanoparticles with pH 8. Firstly, to evaluate the effect of nanoparticle size on fouling development, we used feed solutions containing monodisperse Ludox SM

Table 1
Properties of the hollow fiber MF membrane used [13].

Membrane				
Type	Material	Clean water permeability [L/m^2 h bar]	Pore size [nm]	Zeta potential at pH 8 [mV]
Pentair X-Flow 1.5MF02	PES/PVP	$11.5 \pm 0.5 \cdot 10^3$	200 ± 15	-23.1 ± 2.1

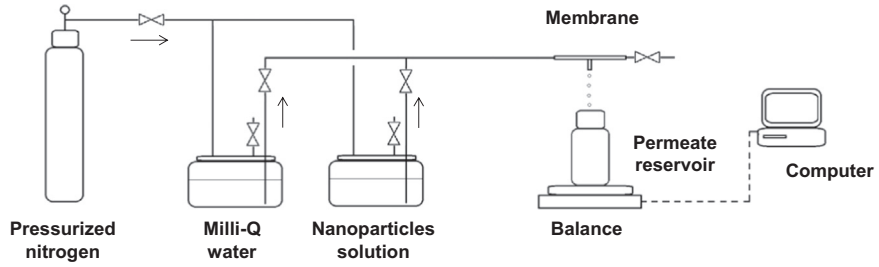

Fig. 2. Flow sheet of the constant pressure filtration setup used.

(11 nm, see Section 3.1), Ludox TM-50 (25 nm, Section 3.1) or Levasil 30/50 (92 nm, Section 3.1) nanoparticles. Secondly, the role of nanoparticle polydispersity was investigated by the filtration of a nanoparticle suspension containing 2 mg/L of binary mixtures of the previously described 11 nm, 25 nm or 92 nm silica nanoparticles in weight ratios 5:1, 1:1 or 1:5. In the result and discussion section we refer to the mixture of 11 nm and 25 nm nanoparticles as 11:25 mixture, to the mixture of 11 nm and 92 nm nanoparticles as 11:92 mixture, and to the mixture of 25 nm and 92 nm as 25:92 mixture.

Initially, we carried out all filtration experiments at a transmembrane pressure of 0.2 bar and at room temperature. The role of transmembrane pressure on fouling and rejection development was investigated by applying lower (0.1 bar) or higher (0.4 bar) transmembrane pressures for filtration of the polydisperse nanoparticle suspensions.

3. Results and discussion

3.1. Nanoparticles

The silica nanoparticles used were analyzed by TEM microscopy. As shown in Fig. 3, the silica nanoparticles in the commercial suspensions vary significantly in their size. From the TEM measurements, for each commercial suspension the size distribution was analyzed. The calculated average number size diameters of the silica nanoparticles are 10.9 ± 1.9 nm, 25.5 ± 5.2 nm and 92.3 ± 14.2 nm for Ludox SM, Ludox TM-50 and Levasil 30/50, respectively. The ratio between the pore size of the membrane (see Table 1) and the nanoparticle diameter is about 18, 8, and 2 for Ludox SM, Ludox TM-50 and Levasil 30/50, respectively.

The characteristics of the nanoparticles used are listed in Table 2. Due to the same surface chemistry and presence of silanol groups [20], the surface of all three nanoparticle types is negatively charged at pH 8 (about -39.9 ± 3.4 mV, -37.7 ± 3.9 mV and -48.7 ± 1.2 mV for Ludox SM, Ludox TM-50 and Levasil 30/50, respectively).

3.2. Filtration experiments

3.2.1. Monodisperse nanoparticle suspensions

The influence of nanoparticle size on fouling development was investigated during constant pressure dead-end microfiltration at pH 8. Feed solutions containing 2 mg/L of silica nanoparticles were prepared by dilution of the commercial nanoparticle suspensions Ludox SM, Ludox TM-50 and Levasil 30/50, which all vary in nanoparticle size (Table 2 and Fig. 3). Fig. 4 shows permeability and rejection data of the investigated silica nanoparticles as a function of the specific permeate volume.

For all three nanoparticle sizes investigated, a decrease in permeability was observed after the introduction of the nanoparticles into the membrane module, as shown in Fig. 4(a). However, the shape of the filtration curve, and therefore the fouling development, varies significantly for each nanoparticle size.

In the case of the smallest (11 nm) Ludox SM nanoparticles, permeability decreases only slightly (about 30%) during the filtration course. A much smaller nanoparticle diameter (see Table 2) than the membrane pore size (see Table 1) allows nanoparticle transport through the membrane without rejection, as shown in Fig. 4(b). For the bigger Ludox TM-50 nanoparticles, having an average diameter of about 25.5 nm (see Table 2), directly at the beginning of the filtration the permeability reduces to 90% of the initial pure water permeability (Fig. 4(a)). Later on, the permeability decreases slowly up to a specific permeate volume of 0.4 m^3/m^2, after which it drastically declines up to about

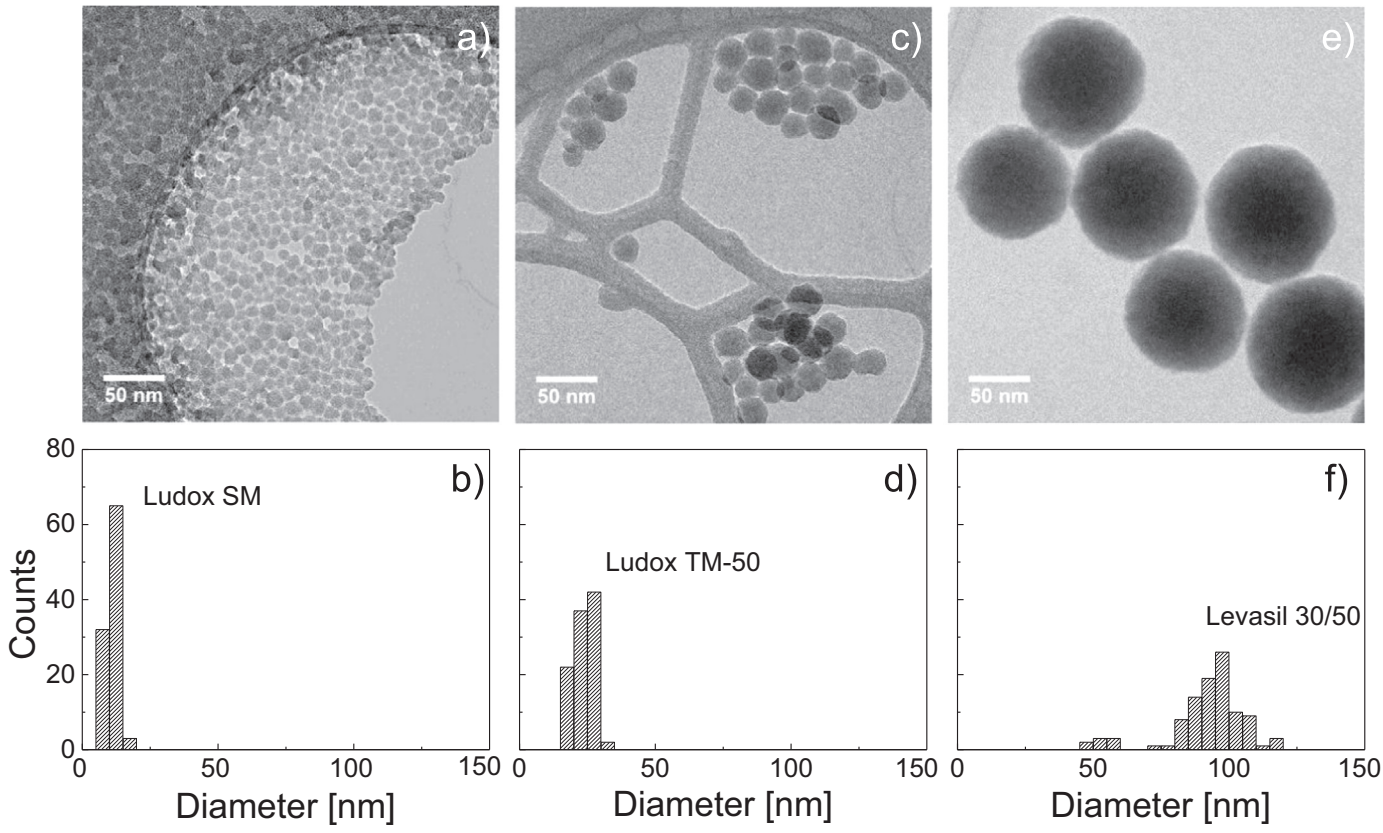

Fig. 3. (a) TEM image and (b) number size distribution of Ludox SM silica nanoparticles, (c) TEM image and (d) number size distribution of Ludox TM-50 silica nanoparticles, (e) TEM image and (f) number size distribution of Levasil 30/50 silica nanoparticles.

0.8 m^3/m^2. In the final filtration phase, the decrease in permeability once again slows down. In the same period, the rejection of the 25.5 nm nanoparticles increases from about 5–90% (see Fig. 4 (b)). Pore clogging and nanoparticle deposition later on leads to the formation of a secondary membrane, which limits nanoparticle transport across the membrane. As described in our previous work [13], the transition from nanoparticle transport to pore blockage is responsible for the concave part of the filtration curve, whereas the evolution from the cake filtration stage to the cake maturation stage is revealed as a convex part of the filtration curve. Such fouling development is characteristic for stable suspensions of nanoparticles having a diameter much smaller than the membrane pore diameter but large enough to be able to block membrane pores. For 92 nm Levasil 30/50 silica nanoparticles (see Table 2), immediately at the beginning of the filtration a fast decline in permeability is observed, as shown in Fig. 4(a). Due to the size of the nanoparticles, which is closer to the membrane pore size, immediate pore blockage occurs resulting in almost 95% nanoparticle rejection already from the beginning of the filtration (see Fig. 4(b)). Interestingly, for 25 nm and 92 nm nanoparticles similar permeabilities and rejections are obtained at the end of the filtration course. These findings suggest that the filtration resistance for both 25 nm and 92 nm nanoparticles is identical, regardless of the size of the particles. However, this is misleading, as different amounts of nanoparticles accumulated on the membrane surface during a single filtration course of both particle sizes. In order to normalize the obtained filtration resistance for the amount of the nanoparticles deposited, in Fig. 5 the filtration resistance is plotted as a function of the accumulated nanoparticle mass. The accumulated nanoparticle mass was calculated from the mass balance using the nanoparticle concentrations in the feed solution and in the permeate samples.

For the 92 nm nanoparticles, due to the high nanoparticle rejection (95%) already from the beginning of the filtration (see Fig. 4 (b)), a large amount of nanoparticles accumulated on the membrane surface (about 3 g/m^2). In the case of the 25 nm nanoparticles, pore blockage was delayed, which postponed the development of the filtration cake and delayed the increase of the nanoparticle rejection to about 90%. Thus, the final accumulated mass of the 25 nm nanoparticles is lower (about 2.3 g/m^2) than that obtained for the 92 nm nanoparticles (about 3 g/m^2). The smallest 11 nm nanoparticles do not clog the pores, and only a very limited amount of the nanoparticles is retained by the membrane and accumulated on the membrane. The slope of the resistance development versus accumulated nanoparticle mass (Fig. 5) is the specific cake resistance α (according to Eq. 4), which quantitatively represents the compaction of the filtration cake. Since the filtration resistance develops much faster with accumulated nanoparticle mass for 25 nm than for 92 nm nanoparticles (see Fig. 5.), the specific cake resistance α is greater for the smaller 25 nm nanoparticles, as listed in Table 3.

The difference in specific cake resistance between the two nanoparticle sizes can be explained by the Kozeny–Carman

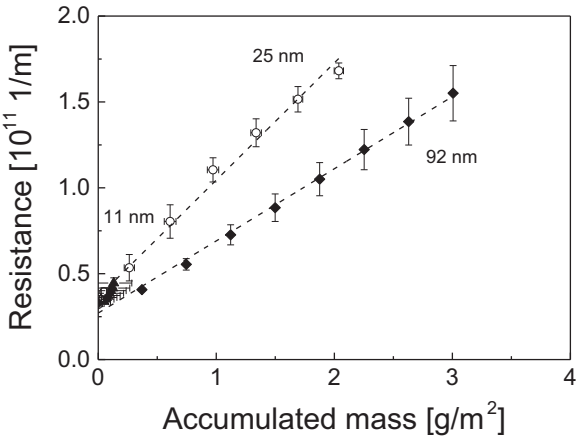

Fig. 5. Filtration resistance as a function of accumulated mass of silica nanoparticles on the membrane for three different nanoparticle sizes (▲ – 11 nm, □ – 25 nm, ◆ – 92 nm).

Table 2
Measured properties of the used silica nanoparticles.

Nanoparticles		
Type	Average diameter [nm]	Zeta potential at pH 8 [mV]
Ludox SM	10.9 ± 1.9	−39.9 ± 3.4
Ludox TM-50	25.5 ± 5.2	−37.7 ± 3.9
Levasil 30/50	92.3 ± 14.2	−48.7 ± 1.2

Table 3
Specific cake resistances and cake porosities obtained during dead-end filtration of monodisperse silica nanoparticles calculated using Eq. (4); n.a. – not available.

Monodisperse nanoparticles	Diameter [nm]	Specific cake resistance α [10^{13} m/kg]	Cake porosity ε
Ludox SM	11	n.a.	n.a.
Ludox TM-50	25	6.8 ± 0.2	0.76 ± 0.01
Levasil 30/50	92	4.3 ± 0.7	0.49 ± 0.02

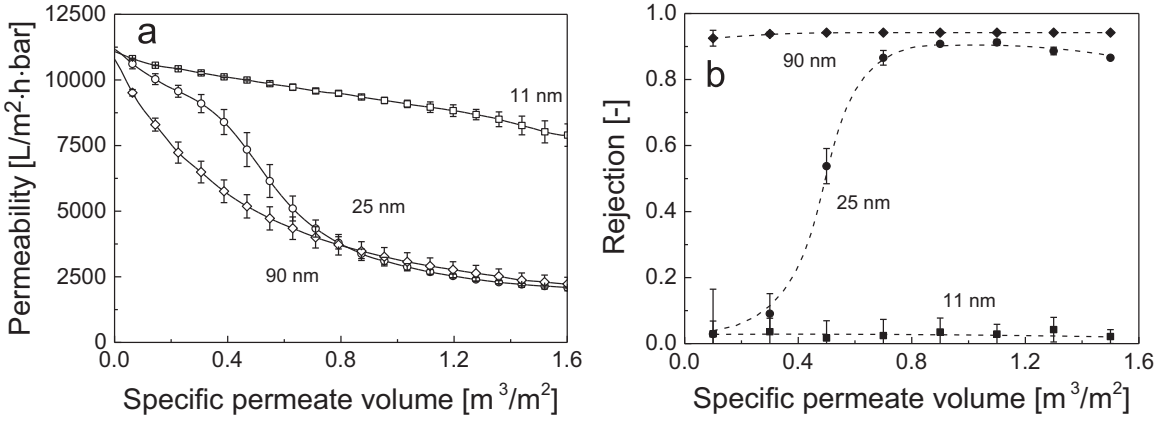

Fig. 4. (a) Permeability and (b) rejection as a function of specific permeate volume for various silica nanoparticle sizes during dead-end microfiltration of 2 mg/L silica nanoparticle suspensions at pH 8.

equation [21] (Eq. 5), which describes the filtration resistance in a porous medium consisting of monodisperse and spherical particles. According to Eq. (5), the filtration resistance of the filtration cake is inversely proportional to the square of the particle diameter. Therefore, for smaller nanoparticles (25 nm) a higher specific cake resistance is expected to be obtained than for larger particles (92 nm), as is indeed shown in Table 3. The results obtained in Fig. 5 were fitted to the Kozeny-Carman equation and the calculated porosities of the filtration cake are listed in Table 3. As shown in Table 3, the filtration cake porosity obtained with monodispersed 25 nm nanoparticles is higher (0.76 ± 0.01) than the porosity of the 92 nm nanoparticles (0.49 ± 0.01). These results are counterintuitive since with a higher specific cake resistance (Table 3) and a slightly lower zeta potential (see Table 2) for the 25 nm nanoparticles compared to the 92 nm particles, we would expect also a lower porosity of the 25 nm particles filtration cake. This is not the case here. We speculate that origin of this unexpected result may be the broader size distribution of 92 nm silica nanoparticles and/or differences in surface properties of 92 nm silica nanoparticles (resulting in a higher Hamaker constant) which allow a lower porosity of the filtration cake despite the higher zeta potential.

3.2.2. *Role of nanoparticle polydispersity: 11 and 25 nm particles*

In this part, we discuss the role of nanoparticle polydispersity on permeability and rejection using 2 mg/L nanoparticle suspensions containing various ratios of 11 nm and 25 nm nanoparticles as an example. For that purpose, feed solutions containing Ludox SM and Ludox TM-50 silica nanoparticles in different ratios were prepared and filtered using the previously described procedure. Permeability decay and corresponding rejection developments are shown in Fig. 6.

Fig. 6(a) shows that the permeability decays obtained for the suspensions containing mixtures of 11 nm and 25 nm nanoparticles lay exactly in between the two filtration curves obtained for the monodisperse nanoparticle suspensions. With increasing concentration of bigger 25 nm nanoparticles, permeability decrease occurs faster due to easier pore blockage. This easier pore blockage at higher 25 nm nanoparticle concentrations results in a faster increase of the nanoparticle rejection, as shown in Fig. 6(b). However, after this sudden rejection increase, for all polydisperse suspensions investigated the rejection stabilizes at a certain maximum level. For feed solutions containing Ludox SM and Ludox TM-50 in ratios 5:1, 1:1 and 1:5, nanoparticle rejection stabilizes at about 40%, 60% and 80%, respectively. McDonogh et al. [16] reported that for charged particles of different sizes, the packing order of the particles is looser and less ordered than for monodisperse nanoparticles. This more porous and less ordered structure of the nanoparticle deposit facilitates nanoparticle diffusion through the filtration cake. Consequently, significantly lower nanoparticle rejections are obtained for polydisperse suspensions than for monodisperse 25 nm nanoparticles. Nevertheless, it is not clear whether the lower rejection is caused by diffusion of smaller nanoparticles through the filtration cake or

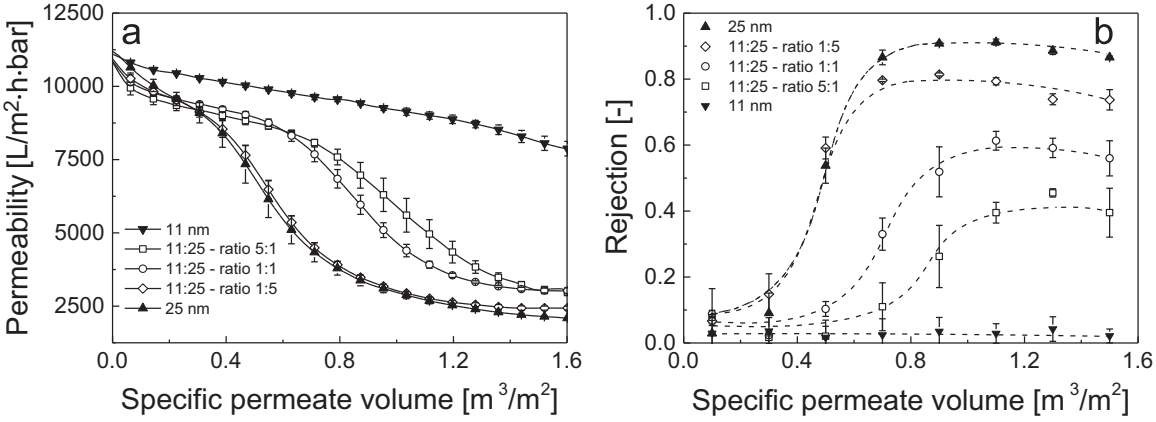

Fig. 6. (a) Permeability and (b) rejection of silica nanoparticles as a function of specific permeate volume for mixtures of 11 nm and 25 nm silica nanoparticles during dead-end microfiltration of 2 mg/L silica nanoparticle suspensions.

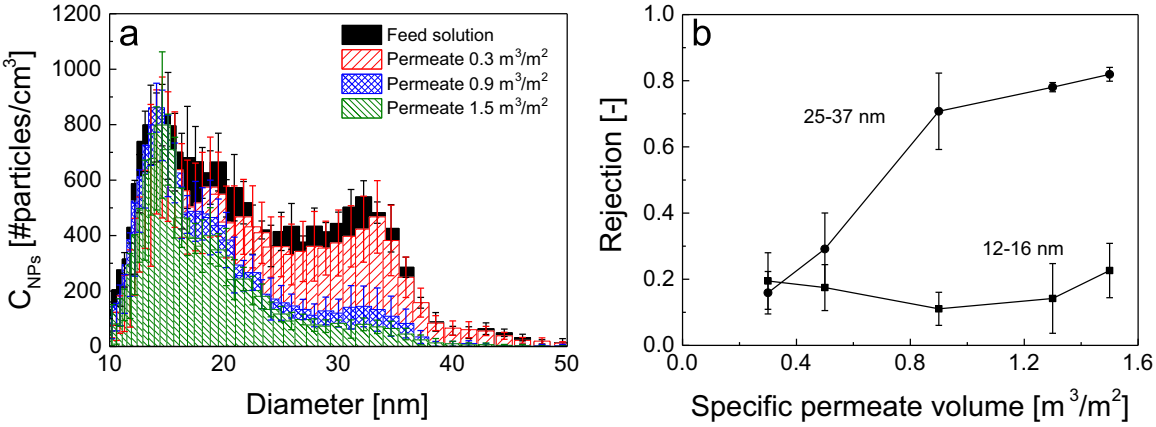

Fig. 7. (a) SMPS size distribution of feed and permeate samples (at three specific permeate volumes) obtained after filtration of a polydisperse suspension of silica nanoparticles; (b) Rejection development of two silica nanoparticle fractions as a function of the specific permeate volume. The 2 mg/L total feed solution was prepared by mixing Ludox SM and Ludox TM-50 in a mass ratio 1:1.

whether it originates from defects in the filtration cake causing both 11 nm and 25 nm nanoparticles to be rejected to a lower extent. To investigate this in more detail, we performed Scanning Mobility Particle Sizer (SMPS) analysis. SMPS of the feed and permeate shows that the nanoparticle size distribution in the feed solutions is different than that of the permeate samples (see Fig. 7 (a)). To quantify these differences, we took the separate data from the fraction of the smaller particles and the separate data from the fraction of the bigger particles, and calculated the rejection for both according to Eq. (2). Although TEM imaging shows that the average particle size of the smaller particles is around 11 and 25 nm, these data stem from particles in the dry state. SMPS data show slightly bigger particle sizes [22]. Therefore, in order to evaluate the rejection of smaller Ludox SM nanoparticles from the data obtained by SMPS, we chose a fraction of nanoparticles with sizes between 12–16 nm. For the larger Ludox TM-50, we considered a representative fraction consists of nanoparticles having a size range between 25 nm and 37 nm. As shown in Fig. 7(b), the fraction of bigger nanoparticles (25–37 nm) is retained much easier than the fraction of the smaller nanoparticles (12–16 nm).

On the one hand, the lower retention of smaller nanoparticles was expected since filtration of monodisperse Ludox SM nanoparticles resulted in a rejection below 10% (see Fig. 4(b)). On the other hand, the deposition of Ludox TM-50 nanoparticles and the pore clogging should form a secondary membrane, which was expected to be less permeable for the small nanoparticles than the original unfouled membrane. We speculate that due to the surface charge of nanoparticles, application of a moderate transmembrane pressure and reduced packing order the filtration cake is highly porous; the distance between nanoparticles in the filtration cake allows preferential transport of smaller nanoparticles through the filtration cake. As a result, overall nanoparticle rejection reduces with a higher concentration of the smaller Ludox SM nanoparticles (Fig. 6(b)). Thus, the higher the concentration of smaller nanoparticles in the mixture, the fewer nanoparticles accumulate on the membrane surface and form the filtration cake. However, regardless of the reduced rejection of the fraction containing smaller nanoparticles (see Fig. 7(b)) their contribution to the reduction of the filtration cake porosity is clear. The specific cake resistance increases with concentration of 11 nm nanoparticles in feed solution, as listed in Table 4. We think that the smaller retained 11 nm nanoparticles can more effectively fill the voids between bigger 25 nm nanoparticles, and by this reduce the porosity of the filtration cake. Consequently, the specific cake resistance increases.

Table 4
Specific cake resistances obtained during dead-end filtration of polydisperse silica nanoparticle suspensions.

Polydisperse nanoparticle mixtures		Specific cake resistance α [10^{13} m/kg]		
Mixture	**Ratio**	**5:1**	**1:1**	**1:5**
11:25		12.5 ± 1.0	8.0 ± 0.7	6.7 ± 0.3
11:92		6.7 ± 0.2	4.7 ± 0.2	4.9 ± 0.1
25:92		6.2 ± 0.3	6.3 ± 0.4	5.3 ± 0.3

3.2.3. Role of nanoparticle polydispersity: larger particles

The difference between membrane pore size and nanoparticle diameter determines rejection and fouling evolution during dead-end filtration, as described before in Section 3.2.1. In general, the bigger the nanoparticles are, the faster the rejection develops due to accelerated pore blockage, and the lower the filtration resistance of the filtration cake is.

Similarly to the results discussed in Section 3.2.2, Fig. 8(a) shows that permeability declines faster when a higher concentration of the larger 92 nm Levasil 30/50 nanoparticles is used in the feed solution. The filtration curve changes gradually from a concave (for 11 nm nanoparticles) to a convex shape with increasing concentration of 92 nm nanoparticles. The transition to the convex shape indicates easier pore blockage of the membrane when a higher concentration of 92 nm nanoparticles is applied. In contrast to the results obtained for mixtures of smaller nanoparticles (11 nm and 25 nm in Section 3.2.2), initial nanoparticle rejection (in the first permeate sample) was more or less proportional to the concentration of 92 nm nanoparticles in the feed solution, as shown in Fig. 8(b). Quantitatively, the measured rejections of silica nanoparticles in the first permeate samples were about 22%, 48% and 77% for mass ratios 5:1, 1:1 and 1:5 of 11 nm and 92 nm nanoparticles in the feed solution, respectively. For 11:92 mixtures, the 92 nm nanoparticles immediately blocked the pores (as it is in the case of monodisperse 92 nm in Fig. 4) forming a filtration cake, whereas for the 11:25 mixtures both nanoparticle fractions initially still could be transported freely through the membrane pores. Furthermore, for the 11:92 mixtures the rejection did not develop that fast and sharp as it did for the 11:25 mixtures, since 11 nm nanoparticles are mainly transported through the filtration cake. Yet, the low retention for 11 nm nanoparticles results in a slight rise of the overall nanoparticle rejection (see Fig. 8(b)) and contributes to an increase of the specific cake resistance (Tables 3 and 4).

The filtration results obtained during dead-end filtration of mixtures containing 25 nm and 90 nm nanoparticles are given in Fig. 9.

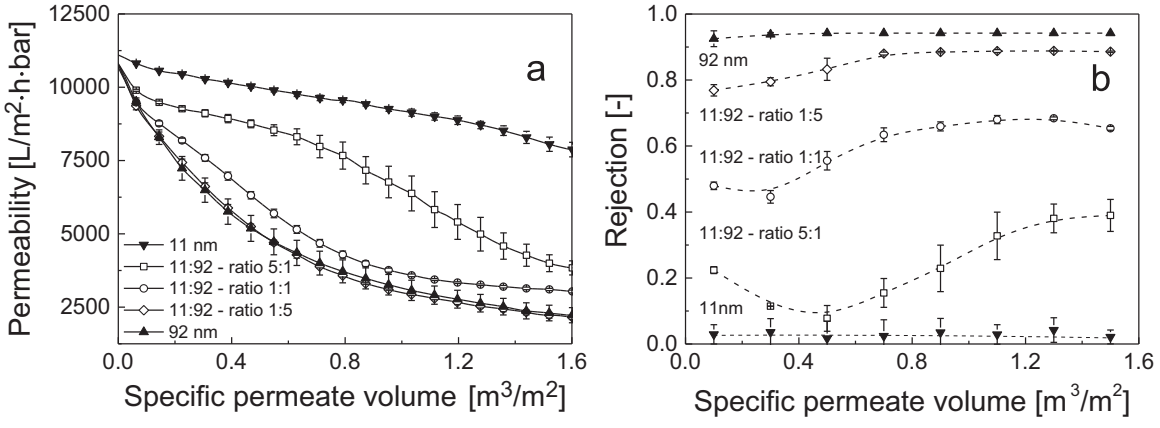

Fig. 8. (a) Permeability and (b) rejection of silica nanoparticles as a function of specific permeate volume for mixtures of 11 nm and 92 nm silica nanoparticles during dead-end microfiltration of 2 mg/L silica nanoparticle feed suspensions.

Similarly to the previous cases, an increased concentration of 92 nm nanoparticles in a feed solution containing also 25 nm nanoparticles results in a faster transition of the concave filtration curve to a convex filtration curve, indicating that pore blockage becomes easier. Moreover, as in the case of 11:92 mixtures, initial rejection of nanoparticles is proportional to the concentration of 92 nm nanoparticles. However, in contrast to the 11:92 mixtures, nanoparticle rejection reached about 90–95% at the end of the filtration for all 25:92 ratios. This high nanoparticle rejection is due to the higher retention of the 25 nm nanoparticles by the filtration cake formed than is the case for the 11 nm particles. As expected also in this case, a higher concentration of 25 nm nanoparticles resulted in densification of the filtration cake, which is expressed as a higher specific cake resistance (Table 4).

3.2.4. Role of transmembrane pressure

The applied transmembrane pressure influences the distance between the deposited nanoparticles in the filtration cake formed, and thus the density of the filtration cake. Repulsive electrostatic interactions between the silica nanoparticles are acting against compaction of the filtration cake by the oppositely directed convective drag force. The applied transmembrane pressure

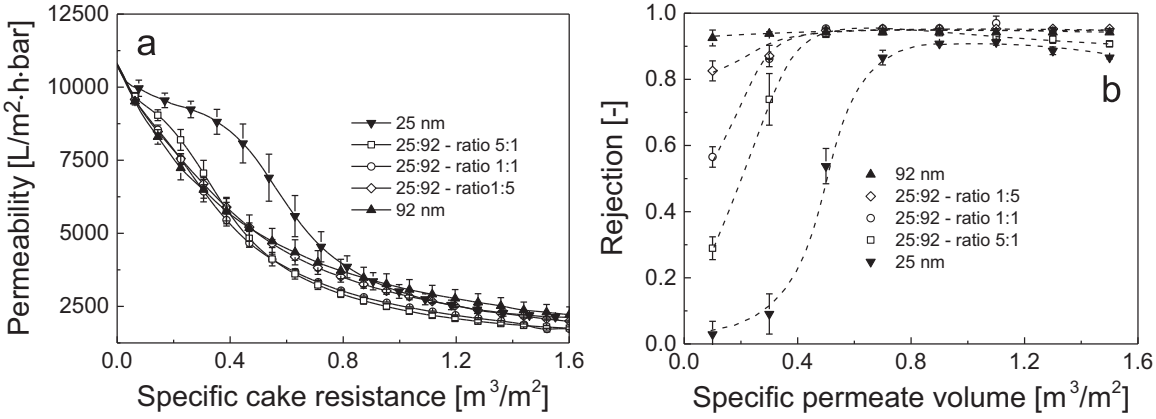

Fig. 9. (a) Permeability and (b) rejection of silica nanoparticles as a function of specific permeate volume for mixtures of 25 nm and 92 nm silica nanoparticles during dead-end microfiltration of 2 mg/L silica nanoparticle suspensions at pH 8.

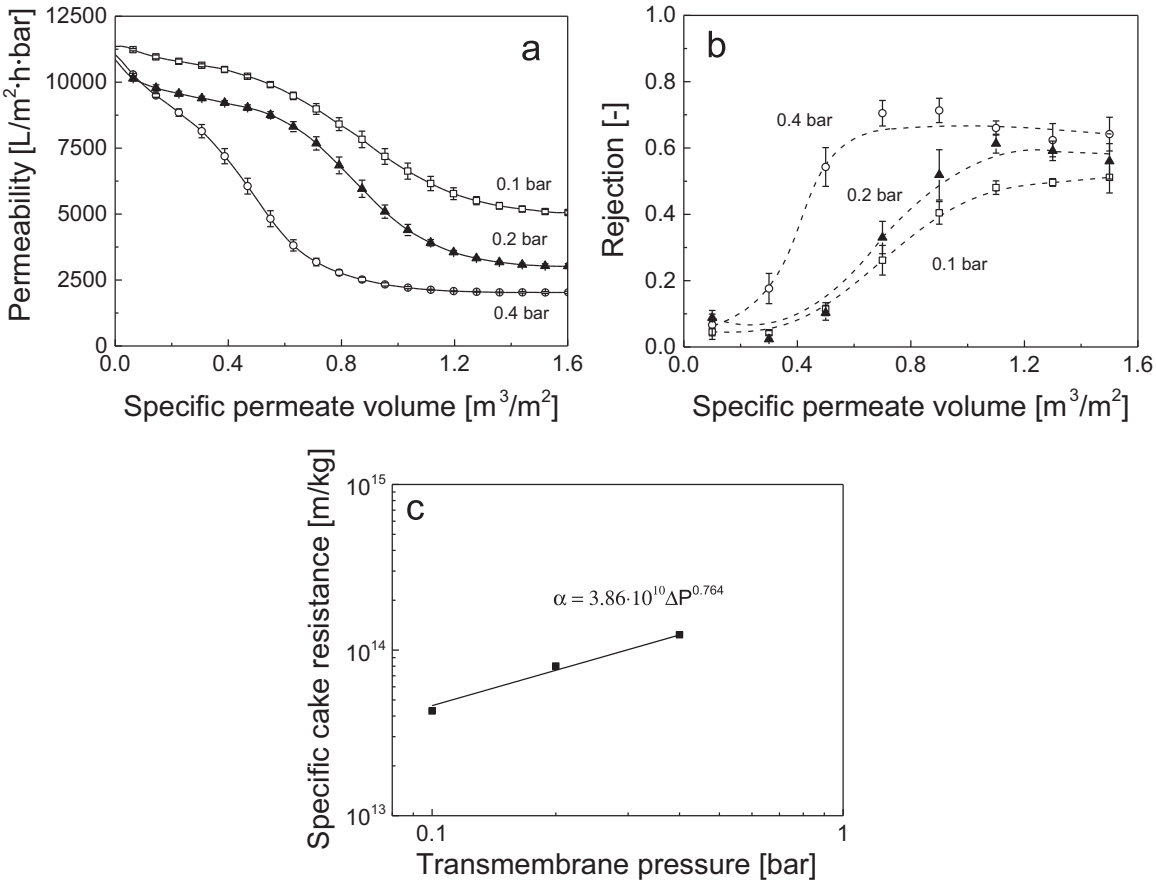

Fig. 10. (a) Permeability and (b) rejection of silica nanoparticles as a function of specific permeate volume and (c) specific cake resistance as a function of transmembrane pressure. Feed solution contained 2 mg/L of 11 nm and 25 nm nanoparticles at mass ratio 1:1 at pH 8.

Table 5
Specific cake resistances obtained during dead-end filtration of a feed suspension containing 2 mg/L of 11 nm and 25 nm silica nanoparticles at mass ratio 1:1 at various transmembrane pressures.

Transmembrane pressure [bar]	Specific cake resistance α [10^{13} m/kg]
0.1	4.3 ± 0.2
0.2	8.0 ± 0.7
0.4	12.4 ± 1.3

determines the permeate flux, which on its turn determines the magnitude of the convective drag force. The role of the transmembrane pressure in fouling and rejection development during filtration of polydisperse nanoparticle suspension was investigated as well. For that purpose, dead-end filtrations of polydisperse silica nanoparticle suspensions were carried out at higher (0.4 bar) and lower (0.1 bar) transmembrane pressures than the reference 0.2 bar used so far. Fig. 10 shows permeability and rejection development of the silica nanoparticle suspensions for different transmembrane pressures. The feed solution used in these experiments contained a 1:1 mixture of Ludox SM (11 nm) and Ludox TM-50 (25 nm) silica nanoparticles.

As expected, an increase of the transmembrane pressure leads to a faster and more severe fouling development. A greater convective drag force at higher transmembrane pressures facilitates nanoparticle aggregation, accelerating pore blockage. This is responsible for the sharp permeability decline in Fig. 10(a) [13]. As a consequence, an increased transmembrane pressure enhances nanoparticle rejection, as shown in Fig. 10(b). Especially, at 0.4 bar this rejection development is much faster than observed for the other two transmembrane pressures used (0.1 bar and 0.2 bar). Already visible from the third permeate sample (0.5 m^3/m^2), Fig. 10(b) shows that due to easier pore blockage, the rejection at 0.4 bar is about 54% in comparison to 10% at 0.1 and 0.2 bar.

After pore blockage, a filtration cake formed on the membrane surface [13]. An indication for its compaction, and thus its contribution to the filtration resistance, is the permeability obtained at the end of the filtration process. As listed in Table 5, for all three transmembrane pressures investigated, the specific cake resistance increases with transmembrane pressure indicating cake compaction. We fitted the obtained specific cake resistances to a power-law function (Eq. 5), as shown in Fig. 10(c). The estimated compressibility coefficient s was about 0.764, proving that the obtained filtration cake is highly compressible [23].

However, as shown in Fig. 10(b), the absolute nanoparticle rejection at the end of the filtration when cake filtration is established [13], increases only slightly with the applied transmembrane pressure. In our case, the nanoparticle rejections measured for the last permeate samples were about 51%, 56% and 64% for 0.1 bar, 0.2 bar and 0.4 bar, respectively. These results clearly show that during cake filtration, nanoparticle rejection increases with the applied transmembrane pressure. However, irrespective of the reduced porosity, nanoparticles could still diffuse through the filtration cake, even at 0.4 bar.

4. Conclusions

In this experimental study we investigated fouling and rejection during dead-end microfiltration of mono- and polydisperse silica nanoparticles much smaller (11 nm, 25 nm and 92 nm and their mixtures) than the membrane pore size (~200 nm). The fouling development of electrostatically stabilized silica nanoparticles is strongly related to the size of the nanoparticles. The bigger the nanoparticles are, the faster pore blockage followed by the cake filtration occurs. When pore blockage happens earlier, a faster increase in nanoparticle rejection is observed. Therefore, an increasing concentration of bigger nanoparticles in a polydisperse suspension results in faster fouling and higher rejections (up to 95%). Nevertheless, the smallest 11 nm nanoparticles were retained only to a low extent in mixtures with bigger nanoparticles, even after formation of the filtration cake. Strong repulsive interactions and moderate transmembrane pressures allow diffusion of the smallest silica nanoparticles through the porous filtration cake. An increase in the transmembrane pressure resulted only in a slight improvement of nanoparticle rejection. The specific cake resistance increases with increasing transmembrane pressure and higher concentrations of smaller nanoparticles in the feed solution. All the conclusions drawn are valid for nanoparticles smaller than the membrane pore size and retained by a surface filtration.

Acknowledgements

This work was supported by NanoNextNL, a micro- and nanotechnology consortium of the government of the Netherlands and 130 partners. We especially acknowledge Vitens N.V. for the ICP-MS measurements. The SMPS research received support from the QualityNano Project (www.qnano-ri.eu) which is financed by the European Community Research Infrastructures under the FP7 Capacities Programme (Grant no. INFRA-2010–262163), and its partner VITO N.V. The authors also thank Evelien Frijns and Jo van Laer from VITO N. V. for their assistance in the SMPS experiments.

References

[1] T.E. Abbott Chalew, G.S. Ajmani, H. Huang, K.J. Schwab, Evaluating nanoparticle breakthrough during drinking water treatment, Environ. Health Perspect. 121 (2013) 1161–1166.
[2] S.F. Hansen, E.S. Michelson, A. Kamper, P. Borling, F. Stuer-Lauridsen, A. Baun, Categorization framework to aid exposure assessment of nanomaterials in consumer products, Ecotoxicology 17 (2008) 438–447.
[3] H. Weinberg, A. Galyean, M. Leopold, Evaluating engineered nanoparticles in natural waters, Trends Anal. Chem. 30 (2011) 72–83.
[4] P. Westerhoff, G. Song, K. Hristovski, M.A. Kiser, Occurrence and removal of titanium at full scale wastewater treatment plants: implications for TiO2 nanomaterials, J. Environ. Monit. 13 (2011) 1195–1203.
[5] K.M. Persson, G. Trägardt, G. Dejmek, Fouling behaviour of silica on four different microfiltration membranes, J. Membr. Sci. 76 (1993) 151–172.
[6] A.I. Schäfer, U. Schwicker, M.M. Fischer, A.G. Fane, T.D. Waite, Microfiltration of colloids and natural organic matter, J. Membr. Sci. 171 (2000) 151–172.
[7] S. Surawanvijit, M. Kim, Y. Cohen, Analysis of membrane filtration efficiency in removal of metal oxide nanoparticles from aqueous nanoparticle suspension in the presence of coagulation pretreatment, clean, Technology (2010) 343–345.
[8] A. Grenier, M. Meireles, P. Aimar, P. Carvin, Analysing flux decline in dead-end filtration, Chem. Eng. Res. Des. 86 (2008) 1281–1293.
[9] W. Guo, H.-H. Ngo, J. Li, A mini-review on membrane fouling, Bioresour. Technol. 122 (2012) 27–34.
[10] Y.S. Polyakov, A.L. Zydney, Ultrafiltration membrane performance: effects of pore blockage/constriction, J. Membr. Sci. 434 (2013) 106–120.
[11] E.M. Tracey, R.H. Davis, Protein fouling of track-etched polycarbonate microfiltration membranes, J. Colloid Interface Sci. 167 (1994) 104–116.
[12] K. Xiao, Y. Shen, X. Huang, An analytical model for membrane fouling evolution associated with gel layer growth during constant pressure stirred dead-end filtration, J. Membr. Sci. 427 (2013) 139–149.
[13] K.W. Trzaskus, W.M. de Vos, A. Kemperman, K. Nijmeijer, Towards controlled fouling and rejection in dead-end microfiltration of nanoparticles – role of electrostatic interactions, J. Membr. Sci. 496 (2015) 174–184.
[14] G. Foley, D.M. Malone, F. MacLoughlin, Modelling the effects of particle polydispersity in crossflow filtration, J. Membr. Sci. 99 (1995) 77–88.
[15] A.E. Contreras, A.S. Kim, Q. Li, Combined fouling of nanofiltration membranes: mechanisms and effect of organic matter, J. Membr. Sci. 327 (2009) 87–95.
[16] R.M. McDonogh, A.G. Fane, C.J.D. Fell, H.-C. Flemming, The influence of polydispersity on the hydraulic behaviour of colloidal fouling layers on membranes: perturbations on the behaviour of the "ideal" colloidal layer, Colloids Surf. A 138 (1998) 231–244.
[17] A.S. Kim, A.N.L. Ng, Hydraulic permeability of polydispersed cake layers: an analytic approach, Desalination 207 (2007) 144–152.
[18] I.W. Lenggoro, B. Xia, K. Okuyama, J.F. de la Mora, Sizing of colloidal

nanoparticles by electrospray and differential mobility analyzer methods, Langmuir 18 (2002) 4584–4591.
[19] S. Chellam, W. Xu, Blocking laws analysis of dead-end constant flux microfiltration of compressible cakes, J. Colloid Interface Sci. 301 (2006) 248–257.
[20] C. Metin, L. Lake, C. Miranda, Q. Nguyen, Stability of aqueous silica nanoparticle dispersions, J. Nanopart. Res. 13 (2011) 839–850.
[21] M. Mulder, Basic principles of membrane technology, 2nd ed., Kluwer Academic, Dordrecht, Boston, 2003.
[22] G. Orts-Gil, K. Natte, D. Drescher, H. Bresch, A. Mantion, J. Kneipp, et al., Characterisation of silica nanoparticles prior to in vitro studies: from primary particles to agglomerates, J. Nanopart. Res. 13 (2011) 1593–1604.
[23] S. Chellam, J. Jacangelo, Existence of critical recovery and impacts of operational mode on potable water microfiltration, J. Environ. Eng. 124 (1998) 1211–1219.